

Generalizable Classification of UHF Partial Discharge Signals in Gas-Insulated HVDC Systems Using Neural Networks

Steffen Seitz, Thomas Götz, Christopher Lindenberg, Ronald Tetzlaff *Senior Fellow IEEE* and Stephan Schlegel

Abstract—Undetected partial discharges (PDs) are a safety critical issue in high voltage (HV) gas insulated systems (GIS). While the diagnosis of PDs under AC voltage is well-established, the analysis of PDs under DC voltage remains an active research field. A key focus of these investigations is the classification of different PD sources to enable subsequent sophisticated analysis.

In this paper, we propose and analyze a neural network-based approach for classifying PD signals caused by metallic protrusions and conductive particles on the insulator of HVDC GIS, without relying on pulse sequence analysis features. In contrast to previous approaches, our proposed model can discriminate the studied PD signals obtained at negative and positive potentials, while also generalizing to unseen operating voltage multiples. Additionally, we compare the performance of time- and frequency-domain input signals and explore the impact of different normalization schemes to mitigate the influence of free-space path loss between the sensor and defect location.

Index Terms—Fault diagnosis, HVDC, partial discharge, neural networks, machine learning.

I. INTRODUCTION

THE increasing integration of renewable energy sources into the existing high-voltage grid requires the use of high-voltage direct current (HVDC) systems. This technology is superior to conventional AC technology for transmitting large amounts of power over long distances because of lower losses, and the elimination of reactive power. Apart from high efficiency, the compact installation of high-voltage equipment is also a critical consideration. Both requirements, high-efficiency power transmission and space-saving installation, are met by gas-insulated systems (GIS), which have been developed for use in transmission systems under AC voltage stress since the 1960s.

A crucial aspect of ensuring fault-free operation in HVDC GIS is the automatic classification of PD-generating defects prior to interpreting the results in terms of fault-free operation [1]. Figure 1 provides a visual representation of an HVDC GIS and illustrates common sources of PDs, including solid metallic particles on the insulation, on free potential or freely moving in the insulating gas, and conducting protrusions on the encapsulation or conductor [2]. In contrast to conventional AC GIS, the number of these devices in operation under DC

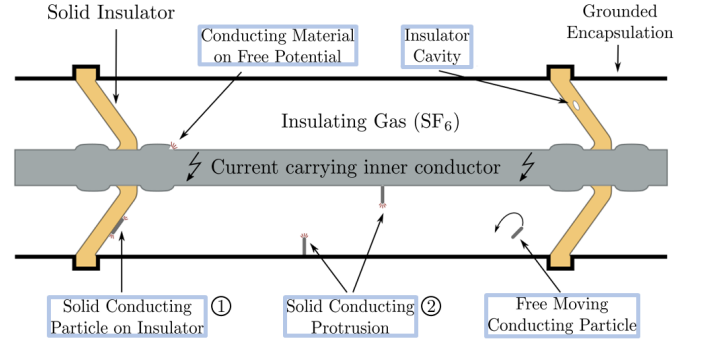


Fig. 1: Schematic representation of a HVDC gas-insulated system and related typical partial discharges generating faults. The presented work aims to classify UHF PD signals caused by particle- ① and protrusion-based ② defects. [2]

stress is rather low. Thus, the measurement [3], classification [4], and physical interpretation [5] of DC PDs continue to be active areas of research. Recently, studies investigating PD development in HVDC GIS indicate that the physical processes responsible for PD formation are the same as compared to those observed under AC voltage stress [6]. However, due to the constant electric field, continuous directed movement of charge carriers, and the generation of space and surface charges, the behavior of DC PDs events, such as amplitude and repetition rate, differs significantly from AC PDs [2].

As a result, the methods and findings related to AC PD classification cannot be directly applied to HVDC GIS. For example, the well-established AC GIS PD detection method, which relies on measurements in the ultra-high frequency (UHF) range and human expert evaluation of phase-resolved partial discharge (PRPD) plots [7, 8], is not suitable for distinguishing DC PD source signals due to the lack of necessary phase information. Consequently, the development and testing of novel DC-specific PD classification methods are essential for ensuring the safety of HVDC GIS.

The most advanced technique for evaluating and identifying PDs under DC voltage stress is pulse sequence analysis (PSA) followed by the assessment of patterns by human experts [9]. This method leverages the amplitude and time information of individual PD events in the UHF signal to identify the underlying defect [10]. However, this approach relies on time-consuming human judgment and it is limited to scenarios with

Steffen Seitz, Christopher Lindenberg and Ronald Tetzlaff are with the Department of Electrical and Computer Engineering, Technische Universität Dresden, 01062 Dresden, Germany. Thomas Götz and Stephan Schlegel are with the Department Electrical Power Systems and High Voltage Engineering, Technische Universität Dresden, E-mail: Steffen.Seitz@tu-dresden.de

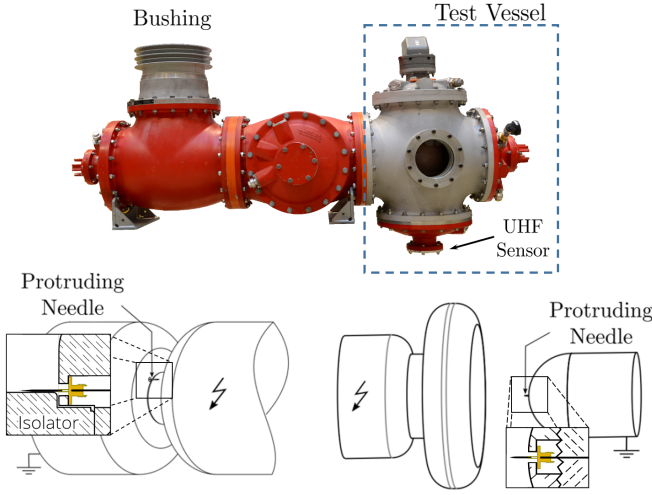


Fig. 2: Picture of the experimental setup (top) and three-dimensional schematics of the electrode arrangements used for the emulation of DC-PD at the gas-solid interface (bottom, left) and at a fixed metallic protrusion (bottom, right) [2].

a single PD source. In situations where multiple sources are active, the PD signals overlap, hindering clear identification and necessitating the use of complex techniques for source separation [11, 12].

To circumvent the time-intensive process of human evaluation, Schober and Schichler [13] proposed a machine learning-based approach for autonomously classifying DC PD signals in GIS. Their novel approach employed Support Vector Machines and MLP to assess PSA features derived from UHF measurements. Despite its promising results, this method inherits the limitations associated with hand-crafted PSA features, such as challenges in classifying signals of multiple active PD sources.

Furthermore, evaluation methods based on neural networks have shown promising results in effectively distinguishing multiple active signal sources in similar domains, when directly applied to time-domain measurements [14, 15]. Consequently, when these techniques are used for DC GIS PD classification, they could potentially eliminate the need for PSA feature evaluation and source separation techniques.

Recently, Beura et al. [16] introduced a first neural network-based method for autonomous feature extraction from UHF time-domain measurements. Their study showed results comparable to the pre-existing PSA methods [13], proving the efficiency of this new approach. However, several critical questions that are essential for the practical application of this method remain open.

First, as already illustrated in Figure 1, DC PDs in GIS originate from multiple sources. Among these source types, PDs generated by particles on the insulator surface are particularly significant [10]. However, the existing literature on PD classification using neural networks based on UHF measurements does not provide sufficient evidence regarding the capability to classify this specific fault type. Moreover, there is a lack of information regarding the classification accuracy of UHF signal-based neural network models specifically for protrusions and insulator particles at both negative and positive

polarities of the inception voltage. This information is crucial for a risk assessment of the asset and a successful transfer of the laboratory experiment results to on-site installations [2].

In addition, previous studies under AC stress have demonstrated that utilizing fast Fourier transform (FFT) coefficients extracted from UHF signals as training data yields improved classification results in similar AC classification tasks [17]. Therefore, it would be advantageous to explore the transferability of these findings to the domain of DC PD classification.

Furthermore, all typical defects of HVDC GIS can experience stress from various multiples of the inception voltage U_i . These individual voltages lead to slightly different discharge patterns [2]. However, the specific U_i at the on-site GIS is not known in practice and creating a suitable amount of data for every combination of the defect type and U_i multiple is impractical for experts. Thus, it is essential to investigate the ability of possible DC PD classification models to generalize from laboratory-based signals to measurements based on unseen U_i multiples of the GIS.

Another challenge in HVDC GIS arises from the amplitude of UHF PD signals, which is influenced by free-space path loss, particularly when the signal has to cross barrier insulators. Thus, the amplitude is proportional to the distance between the defect location and the sensor. As this distance varies in applications outside laboratory tests, it might be advantageous to generally exclude amplitude-related information during model training by applying different normalization methods. In summary, this study contributes to the HVDC GIS PD classification in three significant aspects:

- First, we extend the approach of Beura et al. [16] by providing the missing evidence that a neural network-based architecture can effectively classify DC PD time-domain UHF signals originating from particles on an insulator and fixed metallic protrusions at both negative and positive DC voltage stress. Furthermore, we aim to improve the classification performance by incorporating frequency-domain signals and exploring different layer configurations, including the number, ordering, and hyperparameters (stride, kernel size) of our network.
- Second, we present the first investigation of an HVDC PD classification model in terms of its ability to classify measurements obtained at multiples of the inception voltage U_i that have never been included in the model training. By doing so, we seek to gain insights into the transfer learning capabilities of the model, allowing for generalization from laboratory data to on-site installations under unknown DC voltage stress levels.
- Third, we analyze the impact of different normalization methods on the performance of an HVDC PD classification model to mitigate potential influences of free-space path losses between the sensor and defect locations. This analysis aims to enhance the robustness of the model in real-world scenarios where the distance between the sensor and defect location may vary.

II. EXPERIMENTAL SETUP & METHODS

This study is conducted using UHF DC-PD signals measured under DC voltage stress, as documented in Götz [2] and

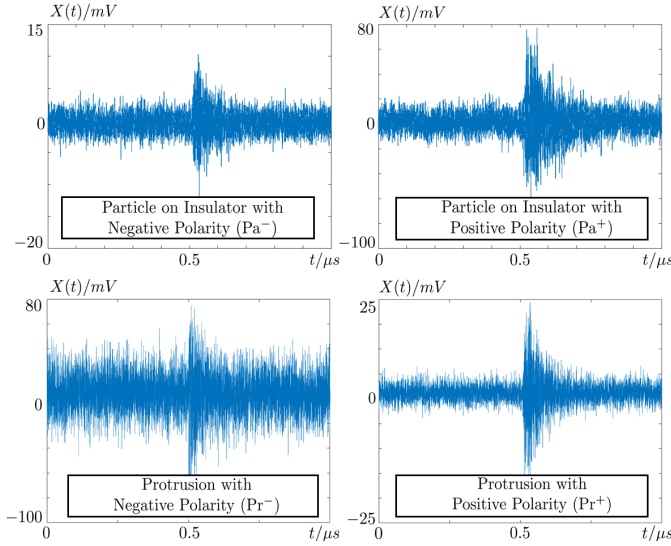


Fig. 3: Time-domain signal examples of the considered defects. Each PD measurement is based on either particles at the gas-solid interface (Pa^- , Pa^+) or protrusions (Pr^- , Pr^+) at negative and positive potential of the needle electrode.

Götz et al. [6]. The measurements were performed in a gas-insulated test setup shown in Figure 2 (top). Similar to Beura et al. [16], model electrode arrays are installed inside a test vessel to simulate the typical behaviour of the defects. The tests were performed using sulfur-hexafluoride (SF_6) as the insulation gas at an absolute pressure of 0.5 MPa.

In the protrusion arrangement (Figure 2; bottom, right), the metallic protruding needle has a length of 5 mm and the needle tip is installed at a distance of 55 mm from the opposing high-voltage electrode. To simulate PD at the gas-solid interface (Figure 2; bottom, left), a 13 mm needle is placed on the surface of an epoxy insulator, typically used in gas-insulated systems. The distance between the needle tip and the opposing high-voltage electrode is 26.7 mm. The high DC voltage with positive and negative polarity up to voltages of 250 kV is applied via the air- SF_6 bushing installed in the centre of the test vessel. PD signals are detected using a standard UHF sensor [18] installed in the test vessel. A 30 dB amplifier is used to increase the signal-to-noise ratio.

The time-dependent PD signals are sampled at 10 GS/s using a Teledyne LeCroy WavePro 735 ZiA digital oscilloscope. Each i -th measurement $M_j = \{s_{j,1}, \dots, s_{j,u}, \dots, s_{j,l_s}\}$, $j \in \{1, \dots, N\}$ has a length of $l_s = 20002$ individual samples $s_{j,u} | s \in \mathbb{R}$, sampled at time step u . The resulting data set contains a total of $N = 33000$ individual PD measurements taken at different multiples of the inception voltage U_i . A so-called source class label is assigned to each M_j based on the defect type, the polarity of the needle and the U_i multiple. Note that the U_i -information is only utilized to investigate the generalization capability of the model (Section III-B). In the classification task the model discards this information and learns to predict the so-called output class labels depicted in Figure 3 based on the given source class measurement. Thus, the output class labels are based only on the defect

type and needle polarity. The number of available source class measurements is shown in Table I.

TABLE I: Number of available measurements M_j of each source class in the dataset of [2].

	Negative Polarity			Positive Polarity		
	$\text{Pa}_{1 \cdot U_i}^-$	$\text{Pa}_{1.5 \cdot U_i}^-$	$\text{Pa}_{3 \cdot U_i}^-$	$\text{Pa}_{1 \cdot U_i}^+$	$\text{Pa}_{1.25 \cdot U_i}^+$	$\text{Pa}_{1.5 \cdot U_i}^+$
Particle	3500	3500	3500	3500	3500	3500
Protrusion	$\text{Pr}_{2 \cdot U_i}^-$	$\text{Pr}_{3 \cdot U_i}^-$	-	$\text{Pr}_{2 \cdot U_i}^+$	-	-
	4000	4000	-	4000	-	-

In each of our experiments, the data is randomly drawn from these recorded measurements and divided into a training and a test set by allocating 80 % of the measurements of each class to the training set D_{train} and the remaining 20 % to the test set D_{test} which are normalized using three different methods.

A. Normalization methods

The objective of data normalization or min-max scaling is to standardize features to a consistent scale. This typically leads to improved performance and training stability of the model. However, dependent on the choice of the method, its application may affect the information contained in the signal. Normalization can be applied in three different ways:

1) *Trainset normalization (Tr)*: In trainset normalization, every sample in each measurement M_j within D_{train} and D_{test} is normalized between -1 and $+1$ according to:

$$\bar{s}_{j,u} = \frac{s_{j,u} - \text{Min}(D_{\text{train}})}{\text{Max}(D_{\text{train}}) - \text{Min}(D_{\text{train}})}. \quad (1)$$

$\text{Min}/\text{Max}(\cdot)$ are operations that return the min-/maximum value of any individual measurement within the dataset. As shown in equation (1), trainset normalization scales each sample in each measurement with respect to the maximum and minimum sample value of all individual measurements across all classes in the dataset. Thus, this method preserves the amplitude information for each measurement in the dataset. However, due to the previously stated free-space path loss problem, it might be advantageous to generally exclude amplitude-related information during model training.

2) *Class normalization (Cl)*: Class normalization scales each sample within a measurement relative to the maximum and minimum sample values of all measurements belonging to the corresponding source class from Table I. In this method, the amplitude-related information is preserved within samples of one class, while it is hidden between measurements of different classes.

3) *Measurement normalization (Me)*: In measurement normalization, each sample in a measurement M_j is scaled based on the maximum and minimum sample values within that specific measurement period in the dataset. In this case, the model can no longer rely on amplitude-related features to classify different samples of class in the dataset.

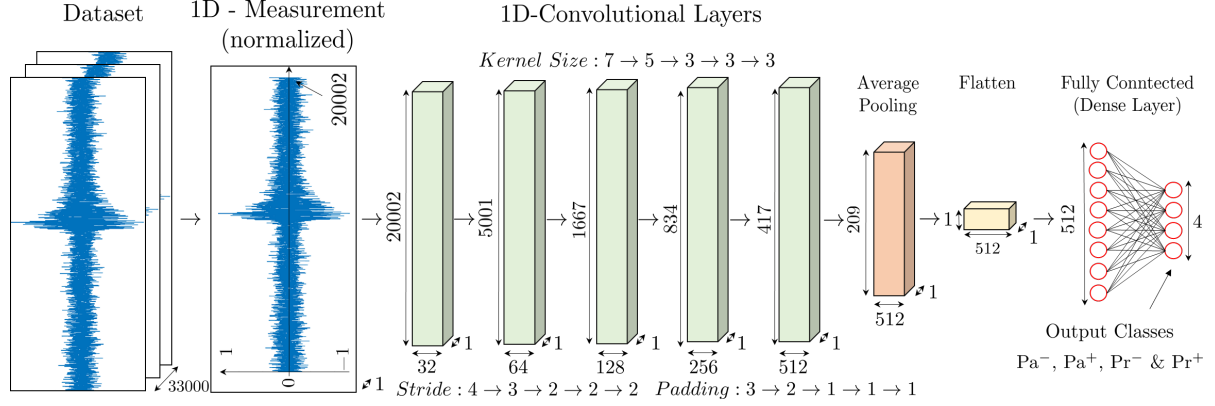


Fig. 4: The proposed model consists of five consecutive 1D-CNN layers with ReLU activation, followed by an average pooling and a flatten layer. The features are fed into a fully connected multi-layer perceptron. This network has 512 ReLU neurons in the input layer and four output neurons with a softmax activation to assign one of the output classes (Pa^- , Pa^+ , Pr^- , Pr^+).

B. Classification model

In our experiments, the normalized UHF amplitude signal measurements and their respective FFT coefficients are separately used to train the neural networks-based model as depicted in Figure 4. These networks use sample measurements and their assigned output class labels in D_{train} to learn their weighting and bias parameters and ultimately predict the correct output class label.

The architecture in our work is based on 1D-convolutional [19] and perceptron layers [20]. We tested different numbers and arrangements of these layer types in conjunction with different activation functions such as ReLU, Sigmoid, and Tanh to achieve an improved classification result. For brevity, only the final model structure is given. This structure and the corresponding activation functions were empirically determined with respect to maximizing classification performance. In the final architecture, the 1D-convolutional layers perform sequential, discrete convolutions between a filter kernel and the data. The extracted features are processed by a ReLU activation function after each layer followed by an average pooling layer and a flattening layer. The data is further processed by the perceptron layer with 512 neurons and a ReLU activation function, which maps the extracted information to the output classes depicted in Figure 3.

The model parameter adjustment is performed using back-propagation and the optimal parameter set is determined by optimizing a cross-entropy loss using ADAM optimization [21]. The initial learning rate of 0.0001 and a batch size of 64 were determined through a random search. In each of our experiments, the network is initialized with 15 different weight initialization seeds to account for the effects of a non-optimal start to the optimization process. The number of individual seeds was chosen to represent a reasonable trade-off between the statistical robustness of the result and the computational time of the model. The performance of each trained model is evaluated using unseen data from D_{test} . In addition, similar to k-fold cross-validation, a different set of measurements from the limited experimental data are randomly assigned to D_{train} and D_{test} in each of the 15 training and testing procedures.

The obtained classification results are averaged to determine a more reliable true positive rate A of the proposed architecture for each defect class. Similarly, the true negative, false negative and false positive rates of the model are determined for all other output classes.

III. EXPERIMENTS & RESULTS

A. Time- and frequency-domain classification results

In this section, we analyze the capability of the proposed architecture to classify unseen measurements of PD generated by a fixed protrusion or a particle adhering to the gas-solid interface. To accomplish this, we utilize UHF signals measured in either the time-domain or frequency-domain at a specific U_i multiple for each output class. In this initial experiment, the baseline dataset D comprises measurements of $\text{Pa}_{1.U_i}^-$, $\text{Pa}_{1.U_i}^+$, $\text{Pr}_{2.U_i}^-$, and $\text{Pr}_{2.U_i}^+$, which are then divided into D_{train} and D_{test} . However, while it would be beneficial to classify the output class based on data measured at the same constant multiple of U_i , for technical reasons the available dataset only contained an unbalanced measurement distribution [2]. As a result, there is an unequal distribution of measurements recorded at the same U_i multiples for each output class, as shown in Table I.

Figure 5 illustrates the confusion matrix of the experiment involving the proposed output classes $\text{Pa}_{1.U_i}^-$, $\text{Pa}_{1.U_i}^+$, $\text{Pr}_{2.U_i}^-$ and $\text{Pr}_{2.U_i}^+$. The model achieves a near-perfect true positive rate A for UHF signals resulting from positive particle (Pa^+) or positive protrusion (Pr^+) defects. For the remaining two output classes, the model obtains only a slightly worse result. In particular, it exhibits a nearly symmetrical confusion between measurements associated with negative particles (Pa^-) and negative protrusions (Pr^-). As mentioned in Section II-B, the model in this experiment was trained separately with 15 different weight initialization seeds. Thus, the presented classification rates of each class in the confusion matrix are the average across all individual runs. The overall performance of the architecture is represented by the average true positive rate \bar{A} . It is determined by averaging the individual true

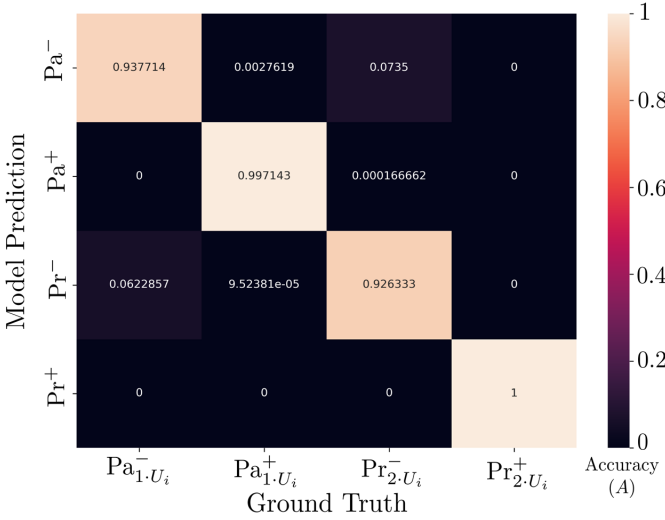


Fig. 5: Model confusion matrix ($\bar{A}_{\text{trainset}} = 0.9653$) obtained by utilizing Pa_{1,U_i}^- , Pa_{1,U_i}^+ , Pr_{2,U_i}^- and Pr_{2,U_i}^+ time-domain measurements, preprocessed by trainset normalization.

positives of all output classes in the confusion matrix. In Figure 5, these values are indicated by the diagonal elements of the matrix, representing the true positive rate of correctly classified PD samples for each class, while the non-diagonal elements represent the false positive and true negative rates when comparing the predicted class against the ground truth.

TABLE II: Average true positive classification rates \bar{A} for different normalization strategies and input datatype.

Input Datatype	Normalization Method		
	Measurement (Me)	Class (Cl)	Trainset (Tr)
Time-Domain (TD)	0.9977	0.9932	0.9653
Freq.-Domain (FFT)	0.9983	0.9975	0.8048

As summarized in Table II, the trained model achieves an $\bar{A}_{\text{Tr}} = 0.9653$ on the trainset normalized measurements in D_{test} . The performance on time-domain test data is generally better if the amplitude information is at least partially- ($\bar{A}_{\text{Cl, TD}} = 0.9932$), or completely- ($\bar{A}_{\text{Me, TD}} = 0.9977$) hidden after normalization. If the time-domain input data is converted to the frequency-domain instead, the classification rate based on the trainset normalized FFT coefficients only achieves an average of $\bar{A}_{\text{Tr, FFT}} = 0.8048$. Thus, if trainset normalization is selected and the model generalization to unseen U_i multiples is not required, time-domain data should be used to train the classifier. Analog to the time-domain signal, the FFT-based true positive rate is higher for class- and measurement normalization. Classifying PDs from the FFT coefficients of the UHF signal resulted in the highest classification performance in our experiments, with $\bar{A}_{\text{Me, FFT}} = 0.9983$. Therefore, the minor difference in performance compared to using the time-domain data hardly justifies the computational cost of converting every measurement to the frequency-domain. Thus, the following experiment relies solely on the time-domain data.

B. Transfer learning experiment results (generalization to an unseen multiple of U_i)

As previously mentioned in Section I, it is important to examine PD classification models in terms of their generalization to measurements of defects recorded at unknown multiples of the GIS inception voltage (U_i). Therefore, each PD measurement is assigned a source class based on the defect type and the inception voltage determined at the time of recording. Note that the exact value of U_i does not need to be further specified, since the approach of this work is centered around the idea of using laboratory data at specific U_i multiples to train a model that generalizes to data from unknown U_i multiples at the on-site GIS.

In the first part of our experiment, we evaluate the generalization performance based on a transfer learning framework, where we pre-train our model based on the data of the same source classes used in Section III-A (Pa_{1,U_i}^- , Pa_{1,U_i}^+ , Pr_{2,U_i}^- and Pr_{2,U_i}^+), to create a baseline for our further studies. Note, that analog to the previous experiment, any measurement is normalized by either trainset-, class- or measurement normalization. After the training process, the generalization performance of the baseline model is assessed by monitoring the model generalization rate G , which is equal to the true positive rate of the model on the untrained $Pa_{1.5,U_i}^+$ measurements in the test set, i.e. $G := A(Pa_{1.5,U_i}^+)$. Note, that the data of $Pa_{1.5,U_i}^+$ is explicitly excluded from the training set in any of the further experiments. herefore, the described measurements are used only at inference time to test the model's generalization to an unseen source class. In this setting, the model can only rely on the knowledge learned from the source class data available in D_{train} to classify any of the $Pa_{1.5,U_i}^+$ measurements in D_{test} .

When trainset normalization (Tr) is used to normalize the baseline dataset (Base), the model achieved a generalization rate of $G_{\text{Tr,Base}} = 0.6801$. With class normalization (Cl), the model achieved a significantly lower result of $G_{\text{Cl,Base}} = 0.4010$, while with measurement normalization, the generalization rate of $G_{\text{Me,Base}} = 0.2085$ did not outperform a random classifier in classifying our four output classes ($G_r = 0.25$). A possible explanation could be the lack of amplitude-related information after data preprocessing with these normalization methods. To investigate this issue further, we refine our basic model by gradually adding measurement data from a previously withheld source class to the trainset D_{train} . The extended training set is used to train the model from scratch. In parallel, the generalization rate of the model is determined after each addition, analogous to the baseline experiment. The sequential training was performed for two different consecutive sequence orders ("Order 1" and "Order 2") to rule out any effects of adding a single record to D_{train} .

The results of this experiment shown in Figure 6 indicate, that the model achieves a generalization rate that is reliably above the baseline results, regardless of the normalization type and sequential ordering, after data from the first additional U_i multiple is added to the baseline dataset. After training the model with data from all available source classes in Table I (except for the $Pa_{1.5,U_i}^+$ data), a generalization performance is achieved that far exceeds random guessing.

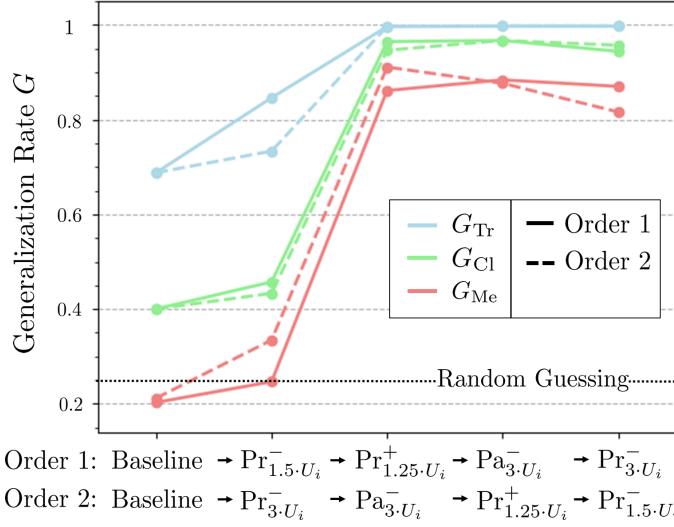


Fig. 6: Model generalization rate G on the untrained U_i multiplier $\text{Pa}_{1.5.U_i}^+$ when additional data from a specific previously withheld source classes is included in the D_{train} . The issue is investigated for trainset (Tr), class (Cl), and measurement (Me) normalization and two different sequential training orders.

Analog to training with a single additional source class, this result is independent of the type of normalization and the sequential order. In contrast to the previous experiment from Table II, trainset normalization performs best in this transfer learning setting. The highest generalization rate with trainset normalization was achieved after training with order 1 (O1), resulting in $G_{\text{Tr}, O1} = 0.9982$. In comparison, the highest generalization rate of class normalization at the end of order 2 (O2) achieved $G_{\text{Cl}, O2} = 0.9578$. The highest measurement normalization based approach only achieves $G_{\text{Me}, O1} = 0.8672$ at the end of order 1. As for the baseline dataset, a possible explanation could be the lack of amplitude-related information after data preprocessing with these normalization methods. In practice, the model is expected to generalize from laboratory measurements to data of a monitored GIS with an unknown U_i multiple. Therefore, assuming negligible effects of free-space path loss, it is recommended to select normalization methods that preserve the amplitude information in the data.

Similar to Section III-A, it is crucial to evaluate model performance concerning the remaining source class measurements from Table I while assessing generalization on the withheld $\text{Pa}_{1.5.U_i}^+$ data. When measurements of all source classes from Table I (except $\text{Pa}_{1.5.U_i}^+$) are included in D_{train} , the model classifies almost all test set measurements correctly. This is illustrated by the confusion matrix in Figure 7. For the sake of brevity, all combinations of normalization methods and training routines are not shown, as they achieved comparable results. In the depicted configuration, the average true positive rate over the available classes in the training set is $\bar{A}_{\text{Tr}, O1} = 0.9979$. When this score is averaged with the associated generalization rate ($G_{\text{Tr}, O1} = 0.9982$), the model attains an average final true positive rate of $\bar{A}_{\text{Tr}, O1} = 0.9977$ for all measurements across all classes in our experiment.

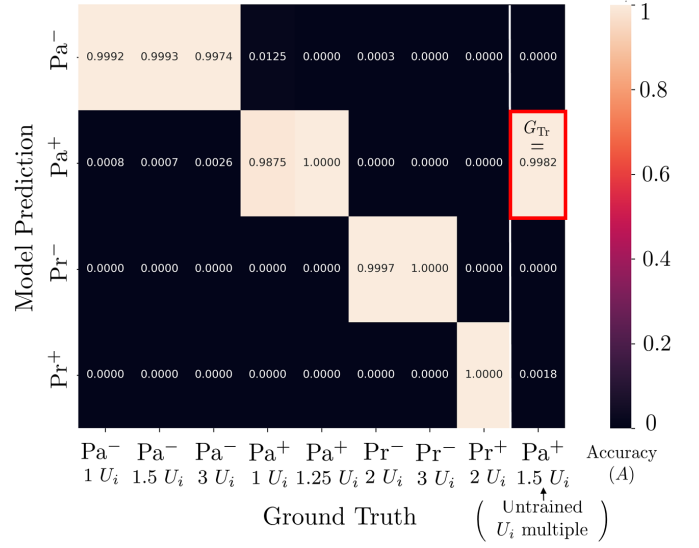


Fig. 7: Confusion matrix and generalization rate G_{Full} (red) of the proposed model. The network was trained using the full trainset-normalized measurements of all available classes from Table I (except $\text{Pa}_{1.5.U_i}^+$), using the train sequence of order 1.

C. Comparison to other methods

Compared to other methods, our model classifies HVDC PDs originating from metallic particles on the gas-solid interface (insulator) (Pa) of a GIS with an average accuracy of 99.67%, which has not been reported in any other non-PSA-based DC PD classification study. In addition, our refined CNN/MLP-based architecture achieves an 1.29% higher average performance than the previous best model in the protrusion (Pr) detection task [16]. The study of Schober and Schichler [13] previously studied Pr and Pa classification, however their PSA-based method did not report individual classification rates for these PD types. In addition, the number of measurements available for each class is very limited, making any comparative analysis on their work even more difficult. Furthermore, our model is the first to differentiate between negative and positive polarities of Pr^\pm and Pa^\pm measurements, while achieving previously unreported generalization capabilities to untrained U_i multiples. Moreover, we are the first to investigate the effect of normalization on the classification performance. The main contributions of our work to the field are summarized in Table III. Note that we excluded approaches based on conventional PSA [9, 10] and PDs under AC [19, 22, 23, 24] from this comparison, as they either depend on time consuming human expert evaluation or rely on measurements of related but different physical phenomena.

IV. CONCLUSION

In this paper, we evaluate the performance and generalizability of a neural network-based method for the classification of DC partial discharges (PDs) at both negative and positive polarity. The ultra-high frequency (UHF) time- and frequency-domain PD signals are generated by conductive protrusions and particles on an insulator. Our study extends the literature on HVDC GIS PD classification in multiple aspects:

TABLE III: Comparison of the presented work to related non-expert-based PD classification approaches in HVDC GIS.

Category	Our work	[16]	[13]
Pr classification accuracy:	99.99%	98.23%	not reported
Pa classification accuracy:	99.67%	not investigated (n.i.)	not reported
Average per class test set size:	733	461	83
No PSA features required:	✓	✓	✗
Defect polarity studied on:	protrusion & solid particle on insulator	particle on free potential	n.i.
Normalization influence	✓	n.i.	n.i.
Generalization to U_i multiples:	✓	n.i.	n.i.

- First, we report the first classification of UHF signals originating from particles adhering to the gas-solid interface (insulators) with an accuracy of 99.67%, without the need for pulse sequence analysis (PSA). Additionally, our model outperforms all previously reported methods by 1.29% on the UHF protrusion signal classification task, achieving an accuracy of 99.99%. The use of frequency-domain signals achieved only a negligible average performance advantage of 0.04% compared to the UHF time-domain signal classification model result which hardly justifies the computational cost of converting each measurement to the frequency-domain.
- Second, we are the first to investigate the transfer learning ability of a UHF signal-based neural network PD classification model to generalize to measurements recorded under unknown DC voltage stress levels. Regardless of the training order, our model correctly classifies 99.87% of the U_i multiple signals not included in the train set as well as 99.77% of all available PD test set measurements.
- Third, we analyze the effect of preprocessing, including sample-, class-, and training set normalization on the performance of a PD classification model in HVDC GIS to mitigate the possible influence of free-space path losses between the sensor- and defect location. Our results show that methods partially eliminating amplitude information perform better in PD classification experiments, while amplitude-preserving methods slightly outperform in the U_i multiple transfer learning task.

In future work, the proposed approach should be applied to measurements of the remaining PD types in HVDC GIS such as insulator cavities, free-moving particles, and material on free potential. We also suggest considering different sensor positions, electrode geometries, and spacing to enhance the methodology. Furthermore, it would be important to study the transfer learning capability on data from additional operating voltages to facilitate the practical application of the method.

ACKNOWLEDGMENTS

This research was partly funded by the German Research Foundation (DFG, project number 379542208) and the German Federal Ministry of Economic Affairs and Climate Action (BMWK, reference: KK5056101KA0). The authors acknowledge the computing time through the ZIH at TU Dresden and the feedback from Thomas Linde and Carsten Knoll.

REFERENCES

- [1] N. Davies and D. Jones, “Testing distribution switchgear for partial discharge in the laboratory and the field,” in *Conference Record of the 2008 IEEE International Symposium on Electrical Insulation*, 2008, pp. 716–719.
- [2] T. Götz, “Partial discharge behaviour of gas-solid insulation systems under DC voltage stress,” Dissertation, Technical University Dresden, 2022.
- [3] A. Abbasi, J. Castellon, A. Cavallini, F. Esterl, and T. Götz, “Progress on partial discharge detection under DC voltage stress,” in *CIGRE Joint Colloquium - SCA2/SCB2/SCD1*, Janpath / New Delhi, 2019.
- [4] Pirker, A. and Schichler, U., “Partial discharges at DC voltage - measurement and pattern recognition,” in *2016 International Conference on Condition Monitoring and Diagnosis*, 2016, pp. 287–290.
- [5] A. Mor, L. Heredia, F. Muñoz, U. Richert, M. Gatzsche, H. He, N. Belda, T. Vu, C. Toigo, and M. Tucek, “Promotion: Progress on meshed HVDC offshore transmission network - report on diagnostic analysis and condition assessment (D15.5).” [Online]. Available: https://www.promotion-offshore.net/fileadmin/PDFs2/D15.5_final_report.pdf
- [6] T. Götz, H. Kirchner, and K. Backhaus, “Partial discharge behaviour of a protrusion in gas-insulated systems under DC voltage stress,” *Energies*, vol. 13, no. 12, 2020.
- [7] N. Achatz, J. Gorablenkow, U. Schichler, B. Hampton, and J. Pearson, “Features and benefits of UHF partial discharge monitoring systems for GIS,” in *Proceedings of 2005 International Symposium on Electrical Insulating Materials, 2005. (ISEIM 2005).*, vol. 3, 2005, pp. 722–725 Vol. 3.
- [8] T. Hoshino, H. Koyama, S. Maruyama, and M. Hanai, “Comparison of sensitivity between UHF method and IEC 60270 for onsite calibration in various GIS,” *IEEE Transactions on Power Delivery*, vol. 21, no. 4, pp. 1948–1953, 2006.
- [9] A. Pirker and U. Schichler, “Partial discharge measurement at DC voltage — Evaluation and characterization by NoDi pattern,” *IEEE Transactions on Dielectrics and Electrical Insulation*, vol. 25, no. 3, pp. 883–891, 2018.
- [10] —, “Application of NoDi* pattern for UHF PD measurement on HVDC GIS/GIL,” Sep. 2019, international Conference on Condition Monitoring, Diagnosis and Maintenance, CMDM 2019 ; Conference date: 09-09-2019 Through 11-09-2019.
- [11] B. Hochbrückner, M. Spiertz, A. Küchler, M. H. Zink, T. Steiner, E. Winkelmann, and K. Backhaus, “Digital filtering methods for interferences on partial discharges un-

der dc voltage,” in *Proceedings of the 21st International Symposium on High Voltage Engineering*. Springer International Publishing, 2020, pp. 560–571.

- [12] B. Hochbrückner, M. Spiertz, M. H. Zink, A. Küchler, and K. Backhaus, “Comparison of algorithms for clustering of partial discharge signals under DC voltage,” in *2019 2nd International Conference on High Voltage Engineering and Power Systems*, 2019, pp. 041–046.
- [13] B. Schober and U. Schichler, “HVDC GIS/GIL - Machine learning algorithms for online PD classification at DC voltage,” in *2022 9th International Conference on Condition Monitoring and Diagnosis (CMD)*, 2022, pp. 225–230.
- [14] B. Adam and S. Tenbohlen, “Classification of multiple PD sources by signal features and LSTM networks,” in *2018 IEEE International Conference on High Voltage Engineering and Application (ICHVE)*, 2018, pp. 1–4.
- [15] S. Adavanne, A. Politis, J. Nikunen, and T. Virtanen, “Sound event localization and detection of overlapping sources using convolutional recurrent neural networks,” *IEEE Journal of Selected Topics in Signal Processing*, vol. 13, no. 1, pp. 34–48, 2019.
- [16] C. P. Beura, P. Wenger, E. Tozan, M. Beltle, and S. Tenbohlen, “Classification of partial discharge sources in HVDC gas insulated switchgear using neural networks,” in *VDE High Voltage Technology; 4. ETG-Symposium*, 2022.
- [17] G. Li, X. Wang, X. Li, A. Yang, and M. Rong, “Partial discharge recognition with a multi-resolution Convolutional Neural Network,” *Sensors*, vol. 18, no. 10, 2018.
- [18] A. Tröger, U. Riechert, S. Burow, and S. Tenbohlen, “Sensitivity evaluation of different types of PD sensors for UHF-PD-measurements,” in *Proceedings of the International Conference on Condition Monitoring and Diagnosis*, 2010.
- [19] S. Seitz, J. Müller, R. Tetzlaff, and P. Holstein, “Neural networks for the classification of electrical discharges,” in *Advances in Acoustics; German Acoustical Society*, 2017, pp. 1019–1021.
- [20] S. Mieruch, S. Demirel, S. Simoncelli, R. Schlitzer, and S. Seitz, “SalaciaML: A deep learning approach for supporting ocean data quality control,” *Frontiers in Marine Science*, vol. 8, 2021.
- [21] D. P. Kingma and J. Ba, “Adam: A method for stochastic optimization,” *CoRR*, vol. abs/1412.6980, 2014.
- [22] W. Wang and N. Yu, “Partial discharge detection with Convolutional Neural Networks,” in *2020 International Conference on Probabilistic Methods Applied to Power Systems*, 2020, pp. 1–6.
- [23] V.-N. Tuyet-Doan, H.-A. Pho, B. Lee, and Y.-H. Kim, “Deep ensemble model for unknown partial discharge diagnosis in gas-insulated switchgears using Convolutional Neural Networks,” *IEEE Access*, vol. 9, pp. 80 524–80 534, 2021.
- [24] E. Gulski and A. Krivda, “Neural networks as a tool for recognition of partial discharges,” *IEEE Transactions on Electrical Insulation*, vol. 28, no. 6, pp. 984–1001, 1993.



in predictive maintenance.

Steffen Seitz received his Diploma (Dipl.-Ing.) degree in electrical engineering from the Technische Universität Dresden in Germany in 2016. He is currently advancing his academic career as a Ph.D. candidate and research associate at the Chair of Fundamentals of Electrical Engineering, under the guidance of Ronald Tetzlaff. His interests include neural network-based condition monitoring and explainable artificial intelligence and explainable artificial intelligence, with a specific focus on enhancing the understandability of model reasoning



Thomas Götz received the Diploma degree in electrical engineering in 2015 and the Ph.D. degree in high voltage engineering in 2022 from the Technische Universität Dresden. From 2015 to 2022 he was a research associate at the Chair of High Voltage and High Current Engineering, where he headed the research group High Voltage Engineering in 2022 and 2023. He is a member of the CIGRE WG D1.63 “Partial discharge detection under DC voltage stress”. One of his journal publications was awarded a national literature award.



Christopher Lindenberg is currently pursuing his B.Sc. degree in Computer Science together with Steffen Seitz and Ronald Tetzlaff at the Technische Universität Dresden in Germany. He is recently researching neural network-based failure diagnosis and condition monitoring at the Chair of Fundamentals of Electrical Engineering.



and Cellular Nonlinear Networks.

Ronald Tetzlaff (Senior Member, IEEE) is the Head of the Chair of Fundamentals of Electrical Engineering, Technische Universität Dresden, Germany. Since August 2020, he is also the Chief Officer of Technology Transfer and Internationalization at the Technische Universität Dresden. His scientific interests include problems in signal and system theory, medical signal processing, stochastic processes, system modeling, system identification, machine learning, mem-elements, memristive systems, Volterra systems, physical fluctuation phenomena,



Stephan Schlegel received the doctoral and the habilitation degree in electrical engineering at the Technische Universität Dresden in 2011 and 2019. He led the research group “Electrical Contacts and Connection” between 2011 and 2020. Since 2020, he is provisional holder of the Chair of High Voltage and High Current Engineering at the TU Dresden. His research focus is in the fields of the fundamentals of the electrical-mechanical-thermal contact behavior as well as the aging mechanisms and long-term behavior of electrical contacts and connections.